IX ECCOMAS Thematic Conference on Smart Structures and Materials
SMART 2019
A. Benjeddou, N. Mechbal and J.F. Deü (Eds)

SUPPRESSION OF DELAY-INDUCED INSTABILITIES OF DIGITAL PIEZOELECTRIC VIBRATION ABSORBERS

G. RAZE[*], A. PAKNEJAD[†], G. ZHAO[†], V. BROUN[‡], C. COLLETTE[†] AND G. KERSCHEN[*]

[*]Space Structures and Systems Laboratory
University of Liège
Allée de la Découverte 9, 4000 Liège, Belgium

[†] Precision Mechatronics Laboratory
Université libre de Bruxelles
Avenue F.D.Roosevelt 50, 1050 Brussels, Belgium

[‡]Département ingénieur industriel
Haute École de la Province de Liège
Quai Gloesener 6, 4020 Liège, Belgium

Key words: Piezoelectric Absorber, Digital Vibration Absorber, Delayed System, Stability

Abstract. Digital piezoelectric vibration absorbers synthesizing passive shunt circuits may be subject to instabilities. This work investigates the cause for these instabilities, and highlights the role of sampling delays in their onset. If for practical reasons the sampling frequency cannot be increased, a stabilization procedure which anticipates the sampling delays is proposed. The theoretical developments in this work are experimentally validated on a piezoelectric beam.

1 INTRODUCTION

Engineering structures from various disciplines tend to be lighter or more slender. This trend usually goes along with smaller structural damping and increased susceptibility to vibrations. This in turn may shorten their lifespan, lower their performance or undermine their safety. Piezoelectric shunt damping is often considered as one potential solution to this issue. It was originally proposed by Forward [1], and formalized by Hagood and von Flotow [2]. The working principle of piezoelectric shunt damping is based on the transduction capability of piezoelectric materials: a piezoelectric transducer is able to convert a part of its mechanical energy into electrical energy. The latter can be dissipated by connecting a so-called shunt circuit to the electrodes of the transducer. A common type of shunt circuit is a resonant one, composed of a resistor and an inductor, arranged either in series or in parallel. The realization of this circuit may be challenging for several reasons. The first one is that the required inductance may be impractically large. A common workaround is to use virtual inductors or girators made up of analog electronics. Designing inductors with high inductances is not impossible though, as demonstrated by Lossouarn et al [3]. However, such components are not widely available and require some expertise to be built. The second reason is that the performance of the piezoelectric shunt is highly sensitive to the values

of the electrical components. Any misevaluation or time-variation of the system characteristics will result in sub-optimal performance, rectified by time-consuming modifications of the electrical parameters.

Fleming et al [4] introduced the concept of synthetic impedance as an alternative solution. The combination of a digital signal processor with a current source makes it possible to realize an arbitrary impedance. The synthetic impedance is an attractive option to realize shunt damping circuits owing to its flexibility. This nonetheless comes at the expense of the need for powering the digital unit and its associated electronics.

It was noted by the authors that instabilities of a system composed of a structure controlled by a synthetic impedance may arise. This work discusses the cause of these instabilities, namely, sampling delays, and proposes a stabilizing methodology. This paper is organized as follows. First, a digital vibration absorber is presented in Section 2. A simplified model is developed in Section 3, and the onset of instabilities is studied. Section 4 proposes a simple stabilization method to suppress these instabilities. The method is experimentally validated on a cantilever piezoelectric beam in Section 5. Finally, conclusions are drawn.

2 DIGITAL PIEZOELECTRIC VIBRATION ABSORBER

Connecting an electrical circuit to the electrodes of a piezoelectric transducer is equivalent to imposing a prescribed relation between the voltage across the electrodes and the current flowing through this transducer. This relation may be described by the impedance (voltage over current) or its inverse, the admittance. From the point of view of the transducer, any circuit which is able to impose this relation is equivalent to the original circuit.

The goal of the digital vibration absorber used in this work is to mimic a piezoelectric shunt circuit by measuring the voltage of a piezoelectric transducer and inject the desired current back into it. The voltage-to-current relation, i.e. the admittance, is programmed into a digital processing unit (DPU). The circuit layout of the digital vibration absorber used in this work is given in Figure 1, which is the same as that used by Matten et al [5].

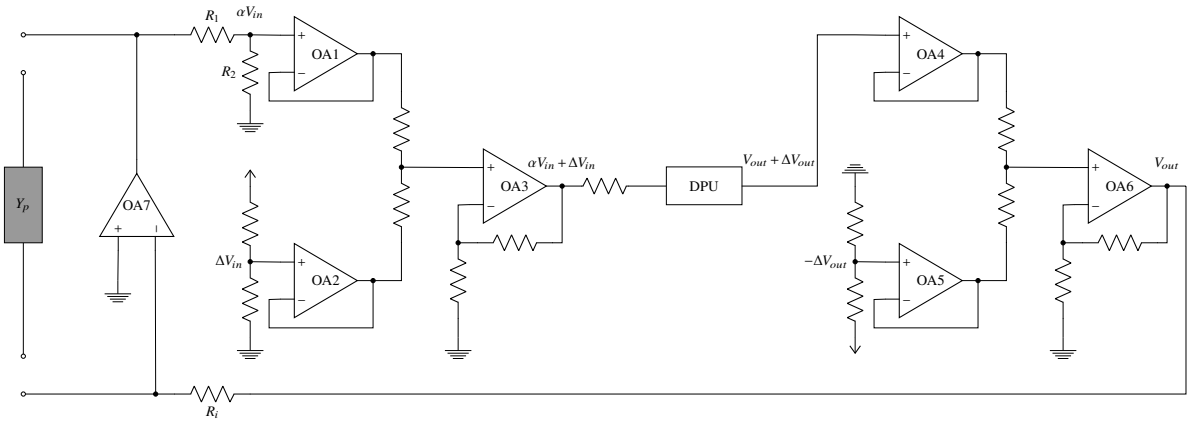

Figure 1: Layout of the digital absorber; the gray box represents a piezoelectric transducer.

The voltage divider composed of R_1 and R_2 is connected to the follower operational amplifier (Op-Amp) OA1, whose output is a scaled-down version of the piezoelectric voltage V_{in} by a factor $\alpha = R_2/(R_1 + R_2)$. OA2 follows a constant offset voltage ΔV_{in} which is added to the input by the summing amplifier OA3 before being fed to the analog to digital converter of the DPU. The DPU computes the

desired input-output relation and outputs via its digital to analog converter a voltage signal $V_{out} + \Delta V_{out}$, which is followed by OA4. A constant negative offset $-\Delta V_{out}$ followed by OA5 is added to the output by the summing amplifier OA6. This signal is applied to one pole of the resistor R_i, while the other is maintained to a virtual ground by OA7. Given the very high input impedance of OA7, the current injected into the piezoelectric transducer is thus V_{out}/R_i.

The input and output offset voltages are generated because the DPU used in this work can only work with positive input and output voltages. They are internally compensated for in the DPU software. An internal gain g is also applied to the transfer function programmed into the DPU for consistency. Indeed, if the desired relation between the piezoelectric voltage V_p and the current I_p is given by H_d, the digital absorber links these two quantities in the following way (assuming that the offsets are perfectly compensated)

$$I_p(s) = \frac{V_{out}(s)}{R_i} = \frac{g}{R_i} H_d(s) V_{in}(s) = \frac{\alpha g}{R_i} H_d(s) V_p(s) \tag{1}$$

where s is the Laplace variable. Assuming for now that the DPU is able to synthesize $H_d(s)$ exactly, a consistency relation is then derived

$$\frac{\alpha g}{R_i} = 1. \tag{2}$$

Typically, g can be computed from the measured values of α and R_i.

3 MODEL OF THE SYSTEM

3.1 Hardware model

The diagram shown in Figure 1 may be simplified while retaining the essential dynamical features of the digital absorber. Because of their large bandwidth (of the order of MHz), the followers and summing amplifiers (OA1 to OA6) are considered as ideal Op-Amps [6]. OA7 is modelled as a differential amplifier with one pole. This leads to the simplified circuit layout shown in Figure 2(a), which can be modelled according to Figure 2(b).

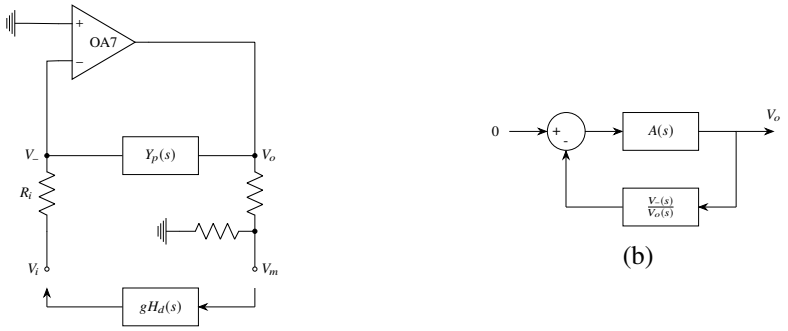

Figure 2: Feedback model of the voltage controlled current injector: simplified circuit layout (a) and equivalent block diagram (b).

From Figure 2(b), the following open-loop transfer function is derived

$$Y(s) = A(s)\frac{V_-(s)}{V_o(s)} = \frac{A_{OL}}{\frac{s}{2\pi f_0} + 1}\frac{V_-(s)}{V_o(s)}, \tag{3}$$

where A_{OL} is the Op-Amp open-loop gain, f_0 is its open-loop bandwidth, V_- is the voltage applied to its inverting input and V_o is its output voltage. Using Kirchhoff's voltage and current laws, the following relation can be derived

$$\frac{V_-(s)}{V_o(s)} = \frac{H_d(s) + Y_p(s)}{\frac{1}{R_i} + Y_p(s)} \tag{4}$$

where H_d is the transfer function synthesized by the DPU and Y_p is the admittance of the piezoelectric transducer, derived in the next subsection.

3.2 Piezoelectric admittance

The system composed of a structure coupled to a piezoelectric transducer may be modelled with the following set of equations

$$\begin{cases} \mathbf{H}_{sc}(s)\mathbf{x}(s) + \gamma\mathbf{B}V_p(s) = \mathbf{f}(s) \\ C_p^{\varepsilon}V_p(s) - \gamma\mathbf{B}^T\mathbf{x}(s) = q_p(s) \end{cases}, \tag{5}$$

where $\mathbf{x}$ is the vector of generalized degrees of freedom, $\mathbf{f}$ is the vector of conjugated generalized forces, $\mathbf{H}_{sc}$ is the structural dynamic stiffness matrix when the piezoelectric transducer is short-circuited, C_p^{ε} is the piezoelectric capacitance at constant strain, $q_p = I_p/s$ is the electric charge flowing through the transducer and $\gamma\mathbf{B}$ is an electromechanical coupling vector [7]. The piezoelectric admittance is then found as

$$Y_p(s) = \left.\frac{sq_p(s)}{V_p(s)}\right|_{\mathbf{f}=\mathbf{0}} = sC_p^{\varepsilon} + s\gamma^2\mathbf{B}^T\mathbf{H}_{sc}^{-1}(s)\mathbf{B}. \tag{6}$$

The dynamic stiffness matrix may be expanded as

$$\mathbf{H}_{sc}^{-1}(s) = \mathbf{\Phi}_{sc}\left(s^2\mathbf{I} + s\mathbf{Z}\mathbf{\Omega}_{sc} + \mathbf{\Omega}_{sc}^2\right)^{-1}\mathbf{\Phi}_{sc}^T \tag{7}$$

where $\mathbf{\Phi}_{sc}$ is the matrix of mass-normalized mode shapes when the piezoelectric transducer is short-circuited, $\mathbf{I}$ is an identity matrix, $\mathbf{Z}$ is a diagonal modal damping matrix and $\mathbf{\Omega}_{sc}$ is a diagonal matrix containing the short-circuit resonance frequencies $\omega_{sc,i}$. The vector of modal strains in the piezoelectric transducer is given by

$$\mathbf{B}^T\mathbf{\Phi}_{sc} = [\phi_1, \cdots, \phi_N]. \tag{8}$$

Equations (6)–(8) give the following modal expansion

$$Y_p(s) = sC_p^{\varepsilon}\left(1 + \frac{\gamma^2}{C_p^{\varepsilon}}\sum_{i=1}^{N}\frac{\phi_i^2}{s^2 + 2\zeta_i\omega_{sc,i}s + \omega_{sc,i}^2}\right). \tag{9}$$

It is not straightforward to obtain the modal strains featured in Equation (9) experimentally. Further simplifying assumptions may be made to facilitate the experimental identification of the piezoelectric admittance. From Equation (5), the dynamic stiffness matrix when the piezoelectric transducer is open-circuited can be found to be

$$\mathbf{H}_{oc}(s) = \mathbf{H}_{sc}(s) + \frac{\gamma^2}{C_p^{\varepsilon}}\mathbf{B}\mathbf{B}^T \tag{10}$$

Equation (10) indicates that $\mathbf{H}_{oc}$ and $\mathbf{H}_{sc}$ only differ by a matrix independent of s. Assuming that this matrix is also diagonalized by the congruence transformation with $\mathbf{\Phi}_{sc}$,

$$\mathbf{\Phi}_{sc}^T\left(\mathbf{H}_{oc}(s) - \mathbf{H}_{sc}(s)\right)\mathbf{\Phi}_{sc} = \frac{\gamma^2}{C_p^{\varepsilon}}\mathbf{\Phi}_{sc}^T\mathbf{B}\mathbf{B}^T\mathbf{\Phi}_{sc} \approx \mathbf{\Omega}_{oc}^2 - \mathbf{\Omega}_{sc}^2 \tag{11}$$

where $\mathbf{\Omega}_{oc}$ is a diagonal matrix containing the open-circuit resonance frequencies $\omega_{oc,i}$. Equating the diagonal entries in Equation (11) leads to the following relation

$$\frac{\gamma^2}{C_p^\varepsilon}\phi_i^2 \approx \omega_{sc,i}^2 K_{c,i}^2 \tag{12}$$

where

$$K_{c,i}^2 = \frac{\omega_{oc,i}^2 - \omega_{sc,i}^2}{\omega_{sc,i}^2} \tag{13}$$

is the square of the effective electromechanical coupling factor (EEMCF) [8]. Inserting Equation (12) into Equation (9), one gets the approximate piezoelectric admittance

$$Y_p(s) \approx sC_p^\varepsilon \left(1 + \sum_{i=1}^{N} \frac{\omega_{sc,i}^2 K_{c,i}^2}{s^2 + 2\zeta_i \omega_{sc,i} s + \omega_{sc,i}^2}\right) \tag{14}$$

Near the resonance frequency of a structural mode, the contribution from non-resonant modes may be neglected provided that the natural frequencies are well-separated. In this case, the piezoelectric admittance may be approximated as

$$Y_p(s)\big|_{s\approx j\omega_{sc,i}} \approx sC_p^\varepsilon \left(1 + \frac{K_{c,i}^2 \omega_{sc,i}^2}{s^2 + 2\zeta_i \omega_{sc,i} s + \omega_{sc,i}^2}\right) \tag{15}$$

3.3 Sampling delays model

The use of a DPU incurs delays associated with the sampling of input and output signals, as well as the clock frequency of the processor. The former (associated with frequencies of the order of kHz) being usually much slower than the latter (associated with frequencies of the order of MHz), only the delays induced by the sampling procedure are taken into account. They are simply modelled by a zero-order-hold operator [9]:

$$H_d(s) = \frac{1 - e^{sT_s}}{sT_s} H(s), \tag{16}$$

where T_s is the sampling time and $H(s)$ is the synthesized transfer function. This model assumes that the DPU is able to compute the output instantaneously from the input, and keeps this output constant for one sampling period.

Now that all the terms involved in the open-loop transfer function (Equation (4)) are known, it is possible to assess the effect of these delays on the performance of the closed-loop system.

3.4 Delay-induced instabilities

As can be seen in Equations (3) and (4), the sampling delays only affect the zeros of the open-loop transfer function. As is well-known in feedback control theory [9], the zeros of the open-loop transfer function are asymptotic positions for the poles of the closed-loop transfer function as the open-loop gain tends to infinity. Hence, knowing their position is of paramount importance to assess the stability of the closed-loop system.

As an illustrative example, Figure 3 compares the poles and zeros of an ideal (i.e. without delays) transfer function and a delayed one. These transfer functions are computed from the characteristics of the experimental system described in Section 5, for which a shunt circuit is synthesized to mitigate the first then the second structural mode.

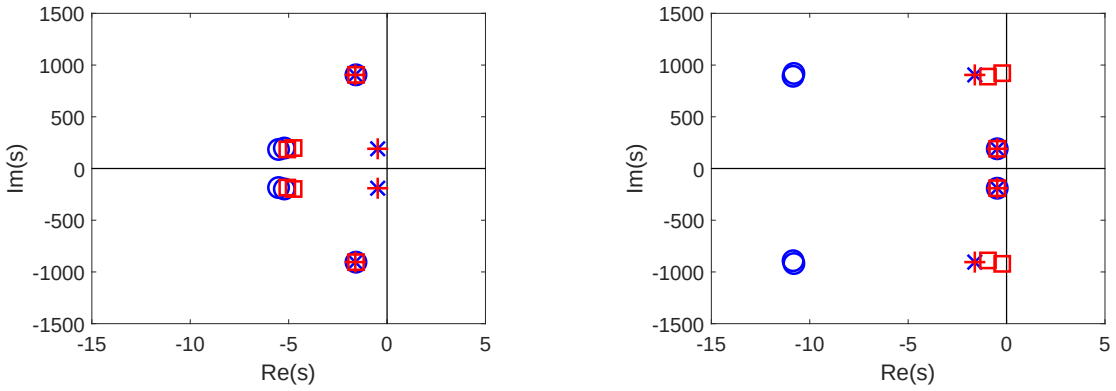

Figure 3: Poles (×) and zeros (○) of an ideal open-loop transfer function, and poles (+) and zeros (□) of a delayed open-loop transfer function: mode 1 (a) and mode 2 (b).

Figure 3(a) indicates that the delays effect is quite low for the first mode, although a small effect is visible on the zeros. In contrast, as seen in Figure 3(b), the delays cause a large shift of the zeros associated with mode 2 toward the right-half of the complex plane. The zeros almost become non-minimum phase, which signifies that the closed-loop system could be conditionally stable. As will be shown in Section 5, this estimate of the zeros is somewhat optimistic, and the closed-loop system is actually unstable.

3.5 Discussion

As the previous Subsection highlighted, the delays induced by the sampling procedure may lead to a destabilization of the vibration absorber, defeating completely its purpose. This destabilization is somewhat counter-intuitive, given that the DPU should synthesize a fully passive circuit, and that the sampling frequency is two orders of magnitude greater than the frequencies of interest. It should however be emphasized that this issue is solely hardware-related. A simple solution to this problem would be to increase the sampling frequency to a high enough value, but this is not always desirable for two reasons.

The first reason is linked to the power consumption of the DPU. The dynamic power consumption of an embedded system can be estimated by [10]

$$P = \beta C_L V_{cc}^2 f_{CPU} \tag{17}$$

where β is the activity factor, C_L is the load capacitance, V_{cc} is the supply voltage and f_{CPU} is the clock frequency at which the DPU is operating. Increasing the sampling frequency will increase β and/or f_{CPU}, leading to a higher power consumption. Moreover, if f_{CPU} is increased, V_{cc} will also have to be increased, which leads to an actual power consumption proportional to f_{CPU}^3 [10].

The second reason is that the DPU sampling frequency may only be increased up to the hardware limits, which may be quickly reached. There could be the possibility to buy more powerful hardware, but the financial cost of such equipment could become prohibitive.

For these reasons, a stabilization method working for a given sampling frequency is proposed in the next section.

4 STABILIZATION PROCEDURE

The model developed in the previous section highlighted the role of sampling delays in the onset of instabilities. In this section, an anticipative method is proposed to cure the instability by placing the zeros of the delayed open-loop transfer function near or at the same location as those of the open-loop transfer function without delays.

The ideal transfer function of a hypothetical DPU without delays may be expressed as a rational transfer function

$$H(s) = \frac{\sum_{n=0}^{N} b_n s^n}{\sum_{m=0}^{M} a_m s^m} \tag{18}$$

and the zeros of the open-loop transfer function without delays satisfy

$$H(z_k) + Y_p(z_k) = 0, \qquad \forall k \in [1, \cdots, K] \tag{19}$$

The stabilization procedure consists in finding the modifications Δa_m and Δb_n to the coefficients a_m and b_n, respectively, such that the modified transfer function given as

$$\tilde{H}(s) = \frac{\sum_{n=0}^{N} (b_n + \Delta b_n) s^n}{\sum_{m=0}^{M} (a_m + \Delta a_m) s^m} \tag{20}$$

synthesized in the DPU give the same zeros as the idealized open-loop transfer function. In other words, the modifications should be such that the following equations are satisfied

$$\tilde{H}_d(z_k) + Y_p(z_k) = \frac{1 - e^{z_k T_s}}{z_k T_s} \tilde{H}(z_k) + Y_p(z_k) = H(z_k) + Y_p(z_k) = 0, \qquad \forall k \in [1, \cdots, K]. \tag{21}$$

Using Equations (18) and (20), this equation becomes

$$\frac{1 - e^{z_k T_s}}{z_k T_s} \frac{\sum_{n=0}^{N} (b_n + \Delta b_n) z_k^n}{\sum_{m=0}^{M} (a_m + \Delta a_m) z_k^m} = \frac{\sum_{n=0}^{N} b_n z_k^n}{\sum_{m=0}^{M} a_m z_k^m}, \qquad \forall k \in [1, \cdots, K]. \tag{22}$$

Carrying simple algebraic manipulations, Equation (22) can be recast into a linear system

$$\mathbf{M}\boldsymbol{\Delta} = \mathbf{r} \tag{23}$$

in which the unknowns are gathered in one vector

$$\boldsymbol{\Delta} = [\Delta a_0, \cdots, \Delta a_M, \Delta b_0, \cdots \Delta b_N]^T \tag{24}$$

and $\mathbf{M}$ and $\mathbf{r}$ are deduced from Equation (22). Usually, $K \neq m + n + 2$ and the system is not square. A simple way of solving Equation (23) is to take its optimal solution in the least-squares sense

$$\boldsymbol{\Delta}^* = \left(\mathbf{M}^T \mathbf{M}\right)^{-1} \mathbf{M}^T \mathbf{r}. \tag{25}$$

The coefficients of a transfer function defined as in Equation (18) can all be multiplied by an arbitrary constant and still represent the same transfer function. This lack of unicity can lead to numerical issues. This can be fixed by setting one of the components of the vector $\boldsymbol{\Delta}$ to an arbitrary value. A simple choice is to choose one of the coefficients to be zero, which amounts to suppressing the corresponding column in the matrix $\mathbf{M}$.

5 EXPERIMENTAL VALIDATION

An experimental validation of the proposed approach is described in this section. A picture of the experimental setup is given in Figure 4. The structure is a cantilever beam with a thin, clamped lamina attached to its free end. The beam is covered with ten pairs of piezoelectric patches along its length. It is excited at midspan by an electrodynamic shaker (TIRA TV 51075) to which is also attached an impedance head (DYTRAN 5860B). An acquisition system (LMS SCADAS MOBILE) is used to record the signals. A more detailed description of the experimental setup can be found in Lossouarn et al [11].

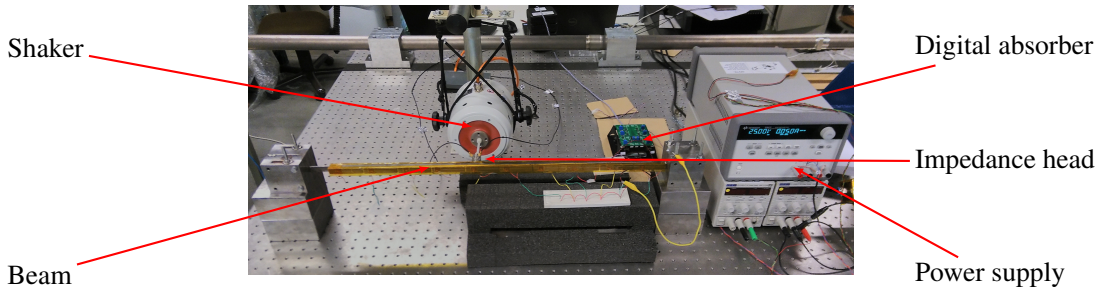

Figure 4: Picture of the experimental setup.

Five of the ten pairs of patches are connected in parallel to the digital absorber. The two first bending modes of the beam are sequentially targeted for shunt damping. To identify the system, the frequency response functions (FRFs) when the patches are short-circuited and when they are open-circuited are measured. These FRFs, noted x/f, are obtained with a low-level broadband excitation and are displayed in Figure 5.

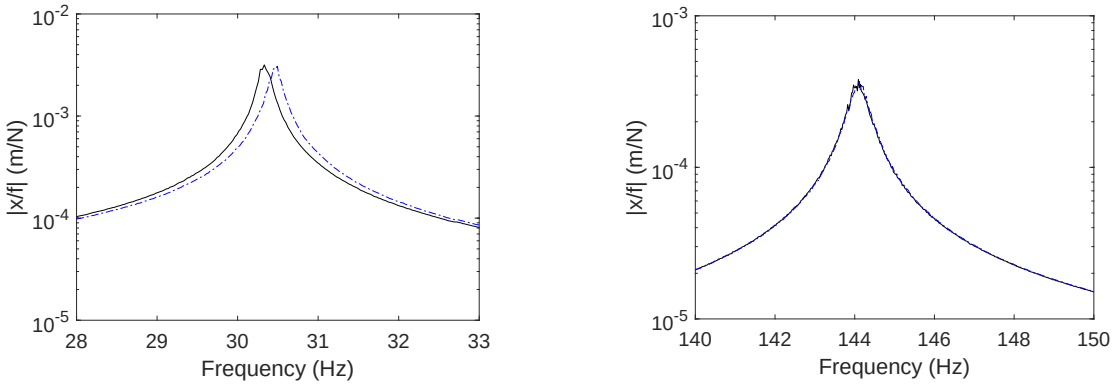

Figure 5: Experimental FRF of the beam when the piezoelectric patch are short-circuited (—) and open-circuited (- - -): close-up on mode 1 (a) and close-up on mode 2 (b).

The short-circuit and open-circuit resonance frequencies as well as the damping ratios are estimated by fitting the FRFs in Figure 5. The piezoelectric capacitance is measured with a multimeter (FLUKE 177). The parameters of the shunt circuit are then computed according to Soltani et al [12]. All these parameters are gathered in Table 1.

The DPU used in the digital absorber is an Arduino Due. The division ratio is given by $\alpha = 0.033$

Table 1: Identified and computed parameters.

Mode	f_{sc} (Hz)	f_{oc} (Hz)	ζ (-)	C_p^{ε} (nF)	L (H)	R (Ω)
1	30.35	30.47	0.24%	257	109.15	2,241.4
2	144.01	144.10	0.17%	257	4.8791	195.97

and the resistance of the current source is measured as $R_i = 265\Omega$. The series RL shunt circuit transfer function, theoretically given by

$$H(s) = \frac{1}{Ls + R} \tag{26}$$

is programmed into the DPU after discretizing it with Tustin's method, with a sampling frequency of $f_s = 10$kHz. The stabilizing method is used assuming that the approximation given in Equation (15) holds since the two modes are well-separated in frequency. The FRFs are compared when the transfer function is unmodified and when it is modified, with the coefficient of the numerator unchanged (i.e., $\Delta b_0 = 0$ is fixed). The open-loop transfer functions and experimentally obtained FRFs of the controlled structure are given in Figure 6, and the modified shunt circuit parameters are given in Table 2. Compared to the values given in Table 1, the synthesized inductances were empirically increased by 2% and 1% for mode 1 and 2, respectively, to obtain FRFs that exhibit equal peaks.

Table 2: Modified shunt circuit parameters.

Mode	$\tilde{L}$ (H)	$\tilde{R}$ (Ω)
1	109.09	2,440.1
2	4.868	395.49

As can be observed with the first mode in Figure 6(a), synthesizing the unmodified transfer function results in an already stable system which behaves as expected. The stabilization procedure brings negligible changes, as can also be observed in Figure 6(c). In contrast, a digitally synthesized shunt circuit for the second mode results in an unstable system, which is cured by the proposed procedure. The instability is confirmed by looking at the structural response in Figure 7: even when the structure is unforced, a significant acceleration is recorded. The system is thus self-excited, and its response is solely bounded thanks to the saturation of OA7. Figure 6(d) and Table 2 indicate that the physical action of the stabilization procedure is to increase the resistance in the shunt circuit, so as to bring the unstable poles back into the left-half complex plane.

6 CONCLUSIONS

Digital piezoelectric vibration absorbers are subject to instabilities caused by sampling delays. In the event of impossibility to increase the sampling frequency, a stabilization procedure was proposed. This method was experimentally validated on a piezoelectric beam. Future works may extend this method to discrete Laplace transforms in order to work directly on the discretized transfer function.

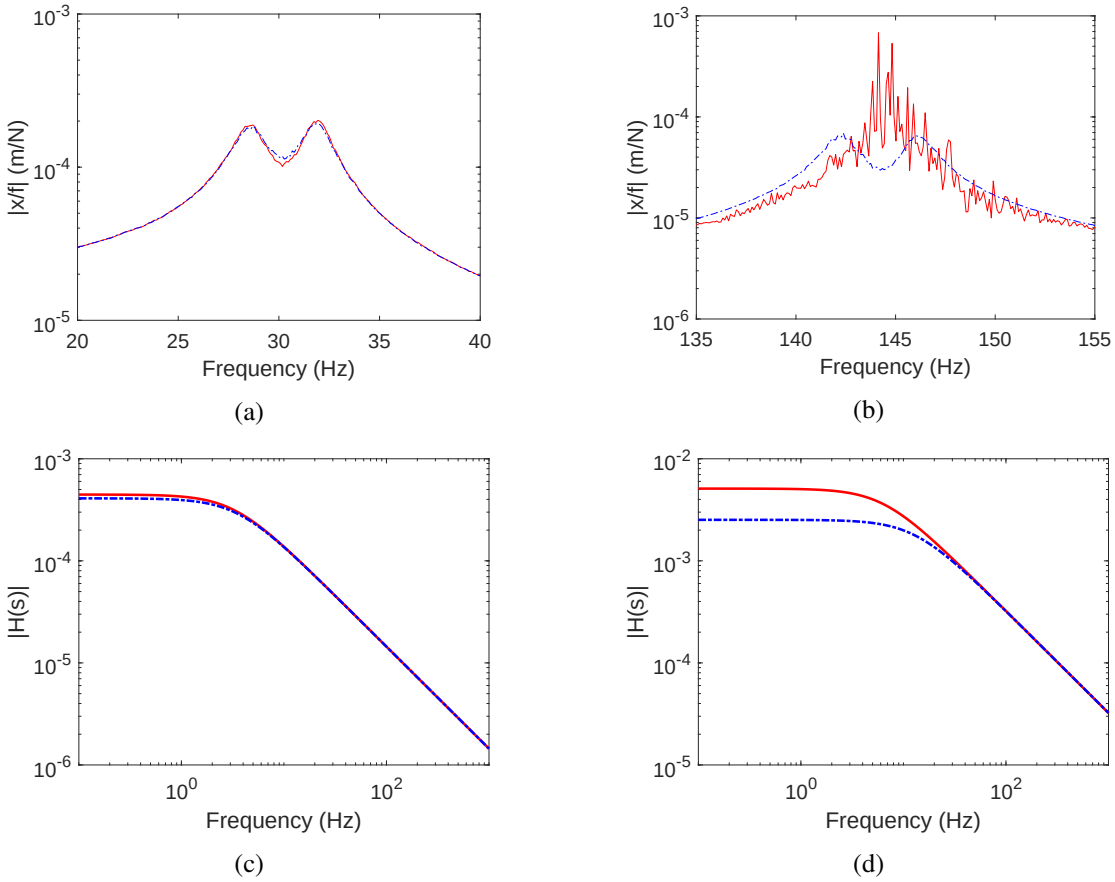

Figure 6: Experimental FRF for mode 1 (a) and mode 2 (b), and synthesized transfer function for mode 1 (c) and mode 2 (d): unmodified transfer function (—) and modified transfer function (- - -).

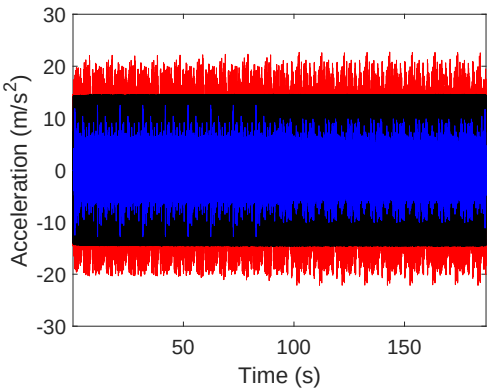

Figure 7: Recorded accelerations with a digital shunt circuit targeting mode 2: unmodified transfer function (—), unmodified transfer function and unforced structure (—) and modified transfer function (—).

7 ACKNOWLEDGEMENTS

The authors would like to acknowledge the financial support of the SPW (WALInnov grant 1610122).

REFERENCES

[1] R. L. Forward, "Electronic damping of vibrations in optical structures," *Applied Optics*, vol. 18, no. 5, p. 690, 1979.

[2] N. W. Hagood and A. von Flotow, "Damping of Structural Vibrations with Piezoelectric Materials and Passive Electrical Networks," *Journal of Sound and Vibration*, vol. 146, no. 2, pp. 243–268, 1991.

[3] B. Lossouarn, M. Aucejo, J. F. Deü, and B. Multon, "Design of inductors with high inductance values for resonant piezoelectric damping," *Sensors and Actuators, A: Physical*, vol. 259, pp. 68–76, 2017.

[4] A. J. Fleming, S. Behrens, and S. O. R. Moheimani, "Synthetic impedance for implementation of piezoelectric shunt-damping circuits," *Electronic Letters*, vol. 36, no. 18, pp. 1525–1526, 2000.

[5] G. Matten, M. Collet, S. Cogan, and E. Sadoulet-Reboul, "Synthetic Impedance for Adaptive Piezoelectric Metacomposite," *Procedia Technology*, vol. 15, pp. 84–89, 2014.

[6] P. Horowitz and W. Hill, *The Art of Electronics*. Cambridge University Press, 3 ed., 2015.

[7] N. W. Hagood, W. H. Chung, and A. V. Flotow, "Modelling of Piezoelectric Actuator Dynamics for Active Structural Control," *Journal of Intelligent Material Systems and Structures*, vol. 1, no. 3, pp. 327–354, 1990.

[8] O. Thomas, J.-F. Deü, and J. Ducarne, "Vibrations of an elastic structure with shunted piezoelectric patches: efficient finite element formulation and electromechanical coupling coefficients," *International Journal for Numerical Methods in Engineering*, vol. 80, pp. 235–268, 2009.

[9] G. F. Franklin, J. D. Powell, and M. L. Workman, *Digital Control of Dynamic Systems*. Addison-Wesley, 1998.

[10] J. M. P. Cardoso, J. G. F. Coutinho, and P. C. Diniz, *Embedded Computing for High Performance: Efficient Mapping of Computations Using Customization, Code Transformations and Compilation*. Morgan Kaufmann, 2017.

[11] B. Lossouarn, J.-F. Deü, and G. Kerschen, "A fully passive nonlinear piezoelectric vibration absorber," *Philosophical Transactions of the Royal Society A: Mathematical, Physical and Engineering Sciences*, vol. 376, p. 20170142, 2018.

[12] P. Soltani, G. Kerschen, G. Tondreau, and A. Deraemaeker, "Piezoelectric vibration damping using resonant shunt circuits: An exact solution," *Smart Materials and Structures*, vol. 23, no. 12, 2014.